

On the High Energy Behaviour of The Total Cross Section in the QCD Dipole Model

Emil Avsar

Institut de Physique Théorique de Saclay, F-91191 Gif-sur-Yvette, France

E-mail: Emil.Avsar@cea.fr

ABSTRACT: In this paper we perform a numerical study of the transverse expansion of hadronic scattering amplitudes in the dipole picture of high energy QCD. We go beyond the mean field approximation by including fluctuations and also wave function saturation effects, and the evolution with both a fixed and a running coupling is investigated. We also study the nonperturbative aspects, and as has been predicted earlier, our results indicate that the Froissart-Martin bound is saturated once confinement effects are included in the evolution. Thus the total cross section increases proportional to the square of the logarithm of the cms energy. Using our proton model developed earlier we furthermore see that we obtain a reasonable value for the proportionality coefficient. The impact of saturation and non-leading effects on this coefficient is also studied.

KEYWORDS: Saturation, Unitarity, Dipole Model, QCD.

Contents

1. Introduction	1
2. The growth of the Black Disc	3
2.1 The BFKL Growth	3
2.2 Saturation Effects in The Cascade Evolution	4
2.2.1 Multiple Scatterings and Boost Invariance	4
2.2.2 Dipole Swing	5
3. Results	9
4. Conclusions	16

1. Introduction

The Froissart-Martin (FM) theorem states that hadronic total cross sections must satisfy

$$\sigma_{tot}(s) \leq C \cdot \ln^2(s/s_0) \text{ as } s \rightarrow \infty, \quad (1.1)$$

where the coefficient C can be estimated as $C \sim 1/m_\pi^2$. The proof of this theorem relies on some general properties such as the unitarity of the S -matrix, the existence of a mass gap, and the possibility of using subtracted dispersion relations. Although not strictly proven within QCD, it is widely believed that this bound should indeed be true for the strong interactions.

The high energy evolution equations (the Balitsky-JIMWLK, or B-JIMWLK hierarchy) for the hadronic amplitudes $T_s(\mathbf{b})$ were derived in [1], and these equations can also be described by the Color Glass Condensate (CGC) formalism [2], or, in the large N_c limit, by the simpler dipole formalism [3]. The solution to these equations exhibits saturation at each \mathbf{b} , *i.e.* $T_s(\mathbf{b}) \leq 1$, with $T_s(\mathbf{b}) = 1$ being the black disc limit. This condition is, however, not sufficient in order to satisfy the FM bound, since the FM bound is relevant for the total cross section which involves an integration over all \mathbf{b} . In fact, it is quite obvious that if one naively takes the solution to the perturbative evolution equations for $T_s(\mathbf{b})$, and then integrates over all \mathbf{b} to get the total cross section as

$$\sigma_{tot}(s) = 2 \int d^2\mathbf{b} T_s(\mathbf{b}), \quad (1.2)$$

one will most certainly violate the FM bound, since the interaction is mediated by massless gluons with a Coulomb like behaviour even at large distances. Indeed for an interaction

mediated by a massless particle, such as the photon in QED, the coefficient C in (1.1) is infinite, since $m_\gamma = 0$.

In this paper we will study the behaviour of hadronic cross sections with respect to the FM bound. We will use our model developed in [4–6], which is based on the QCD dipole model, to calculate the growth of the total pp cross section. In [5] we have suggested the dipole swing mechanism in order to take into account the missing saturation effects in the dipole cascade evolution, and results show that we obtain an almost frame independent evolution. As we will later discuss in section 2.2, the dipole swing has some similarities with the saturation mechanism in the CGC formalism. Furthermore, the swing affects the expansion of the dipole cascade in the transverse plane, and it is therefore interesting to see how large effects it has on the transverse expansion of the scattering amplitude.

Our main results are presented in section 3. We will see that the confinement mechanism is crucial in order to obtain sensible results. This is especially the case when a running coupling is used. Obviously this is to be expected, as otherwise the cascade evolution favours the formation of too large dipoles. Without confinement the cross section grows exponentially in Y (defined as $Y = \ln(s/s_0)$, with $s_0 \approx 1 \text{ GeV}^2$), as expected from the long ranged nature of the massless gluon fields.

The leading order cascade evolution is strongly suppressed by the non-leading effects [6]. Besides the running coupling, the non-leading effects come from the non-singular terms in the gluon splitting function $P(z)$, and the so-called energy scale terms which are related to the conservation of p_+ and p_- respectively [6] (exact energy-momentum conservation goes beyond the NLO corrections, however). Once these effects are included (using the prescription described in [4]), we see that the growth of the cross section is much reduced. Nevertheless, when increasing the energy, one can see that the growth is still faster than what is permitted by the FM bound. Interestingly, we will in this case see that σ_{tot} can be fitted rather well by a polynomial in Y , for $\alpha_s = 0.2$ and Y up to around 32 units.

As the running coupling is a non-leading effect, it might seem strange that the growth of the cross section is much faster as compared to the fixed coupling case. This is mainly due to two reasons. First, the value of α_s gets very large during the evolution (especially in the specific model which we use), signaling the breakdown of the perturbative approach. Secondly, the total growth is faster due to unrealistically large contributions from larger b . However, the growth of $T_s(b=0)$ is actually slower in the running coupling case.

The transverse expansion of the dipole cascade is of course not really consistent with QCD at distances larger than the confinement scale, since it is driven by Coulomb fields. We will therefore also study the expansion when confinement effects are modeled by replacing the Coulomb propagators, $1/\mathbf{k}^2$, with screened propagators, $1/(\mathbf{k}^2 + M^2)$. In this case a $\ln^2 s$ growth is obtained, and the FM bound is thus saturated. We also see that we get a very sensible result for the coefficient C in (1.1). The fact that C can be estimated by combining the perturbative growth with nonperturbative initial conditions has been proposed in [7], although the leading order BFKL result gives a way too large value for C .

2. The growth of the Black Disc

Let us consider a hadronic projectile impinging on a hadronic target. The projectile might here be an elementary colour dipole, and the target a proton or a nucleus. We will from now on denote the generic scattering amplitude between an arbitrary projectile and an arbitrary target by $T_Y(\mathbf{b})$. When the initial (at $Y = 0$) projectile or target is fixed we also use additional parameters to denote the amplitude. For example if the initial projectile is a dipole of size r which scatters off an arbitrary target, then we write $T_Y(\mathbf{r}, \mathbf{b})$. If we have the scattering of two dipoles r and r_0 we instead write $T_Y(\mathbf{r}, \mathbf{r}_0, \mathbf{b})$. The region in \mathbf{b} where the scattering amplitude $T_Y(\mathbf{b})$ satisfies $T_Y(\mathbf{b}) \approx 1$ is called the black disc region, since in this case the projectile is strongly absorbed by the target. The region where $T_Y(\mathbf{b}) \approx 0$ is on the other hand referred to as the “white” region¹ since here the target appears transparent. In the region between, the scattering is “grey”. Specifically, the black disc region is defined as the radius of the disc² within which the average amplitude satisfies

$$T_Y(\mathbf{b}) \geq a \text{ for } |\mathbf{b}| \leq R_{bd}(Y), \text{ where } a \approx 0.5. \quad (2.1)$$

The total cross section can then be estimated as

$$\sigma_{tot}(Y) = 2 \int d^2\mathbf{b} T_Y(\mathbf{b}) \sim 2\pi R_{bd}^2(Y), \quad (2.2)$$

where $R_{bd}(Y)$ is the radius of the black disc at rapidity Y . (Obviously $R_{bd}(Y)$ is also dependent on the projectile and the target, but we do not explicitly write this dependence.) If σ_{tot} is to satisfy the FM bound, it is seen that $R_{bd}(Y)$ can at most grow linearly with $Y = \ln(s/s_0)$. In what follows, we will study the Y dependence for $R_{bd}(Y)$ for different situations, using our model developed in [4–6].

2.1 The BFKL Growth

The Y dependence of $R_{bd}(Y)$ which follows from the solution to the non-linear QCD evolution equations have been discussed in [7–10], in the context of the Balitsky–Kovchegov (BK) equation [1, 11] which is a mean field version of the B-JIMWLK hierarchy. A detailed numerical study of the BK equation with impact parameter dependence was performed in [12]. These works have demonstrated that the BK equation leads to an exponential growth of $R_{bd}(Y)$, even if one starts with an initial profile in \mathbf{b} which falls off very steeply. Using the dipole language, the fast growth of $R_{bd}(Y)$ can be understood as follows. Assume that, for a given dipole projectile of size r , one studies the evolution for $b \equiv |\mathbf{b}| \gg R_{bd}(Y)$, where $T_Y(\mathbf{r}, \mathbf{b}) \ll 1$. The BK equation can then be replaced by the linear BFKL equation³ whose solution in \mathbf{b} can be written as

$$T_Y(\mathbf{r}, \mathbf{r}_0, \mathbf{b}) = \int d^2\mathbf{b}' \int \frac{d^2\mathbf{r}'}{2\pi r'^2} n_Y(\mathbf{r}', \mathbf{b}', \mathbf{r}_0) T_0(\mathbf{r}, \mathbf{b}|\mathbf{r}', \mathbf{b}'), \quad (2.3)$$

¹The white region can be defined as the region where the scattering between a dipole of arbitrary size and the target is small, *i.e.* where the local saturation scale $Q_s(\mathbf{b})$ is smaller than, or the order of, Λ_{QCD} [7].

²The average amplitude is isotropic in the transverse plane. On an event-by-event basis, however, there is no isotropy.

³Strictly speaking one has to be careful when linearizing the BK equation since there might be contributions to the evolution from inside the black region where the scattering is strong, for details see [7, 8].

where n_Y is the dipole density of the target at Y , and T_0 is the basic dipole–dipole scattering amplitude. Here we have assumed that the target initially consists of a single dipole of size r_0 . Of course one could imagine more complicated initial conditions for the target, but as long as the scattering is weak, the precise choice should not matter. The elementary dipole–dipole scattering amplitude, T_0 , can be simplified when the separation of the dipoles are large compared to their sizes (remember that we assume $b \gg R_{bd}$), in which case it decays as $1/|\mathbf{b} - \mathbf{b}'|^4$. It can then be shown that

$$T_Y(\mathbf{r}, \mathbf{r}_0, \mathbf{b}) \sim \alpha_s^2 r^2 n_Y(r, b, r_0) \sim 32\alpha_s^2 \frac{\log \frac{16b^2}{r_0 r}}{(\pi c^2 Y)^{3/2}} \exp\left(\omega Y - \log \frac{16b^2}{r_0 r} - \frac{\log^2 \frac{16b^2}{r_0 r}}{c^2 Y}\right). \quad (2.4)$$

Here $\omega = 4\ln 2 \cdot \alpha_s$, $c^2 = 14\zeta(3)\bar{\alpha}$, and $\bar{\alpha} \equiv \alpha_s N_c/\pi$. Omitting constants and the slowly varying prefactors, we can write

$$T_Y(\mathbf{r}, \mathbf{r}_0, \mathbf{b}) \sim \frac{r_0 r}{b^2} \exp\left(\omega Y - \frac{\log^2 \frac{16b^2}{r_0 r}}{c^2 Y}\right). \quad (2.5)$$

Using definition (2.1), it can now easily be seen that this formula implies an exponential growth for $R_{bd}(Y)$, simply because the power-like decay in b , coming from the Coulomb fields associated with the exchanged gluons, is too slow to compensate for the fast growth in Y .

2.2 Saturation Effects in The Cascade Evolution

2.2.1 Multiple Scatterings and Boost Invariance

The discussion so far has neglected saturation effects in the dipole cascade evolution. In the dipole model, unitarization at each \mathbf{b} is obtained by taking into account multiple dipole interactions. In an eikonal approximation the multiple scatterings can be summed to all orders, with the result that T can be written as

$$T_Y(\mathbf{b}) = \left\langle 1 - \exp\left(-\sum_i \sum_j T_0(\mathbf{x}_i, \mathbf{y}_i | \mathbf{u}_i, \mathbf{v}_i)\right) \right\rangle. \quad (2.6)$$

Here the brackets denote averaging over different events (notice that it is the event by event amplitude which exponentiates). The sums over i and j just denote sums over the dipoles in the individual dipole cascades, and the \mathbf{b} and Y dependences are implicit in the right hand side. Thus we explicitly have $T_Y(\mathbf{b}) \leq 1$ at each \mathbf{b} . This condition is absolutely necessary for our discussion, as otherwise it would make no sense to talk about the black disc limit or the Froissart bound. The Froissart bound determines how rapidly the black disc can expand in \mathbf{b} , but if T is not bounded by 1 then there is no black disc limit at all.

Even though one can unitarize T at each \mathbf{b} , the evolution of the individual dipole cascades satisfy the linear BFKL equation. Since what appears as multiple scatterings in one frame will appear as saturation effects in the cascade evolution (*i.e.* in the onium wavefunction) in another frame, the formalism is not frame independent. The discussion

above should therefore be generalized to the case including saturation effects also in the cascade evolutions. Our results presented below includes such effects, and we therefore discuss them in this section.

2.2.2 Dipole Swing

We have previously argued that one can take into account saturation effects in the dipole cascade evolution by including the so-called dipole swing into the formalism. We will here once again discuss the idea behind the swing. An analytical proof for boost invariance is, however, still lacking. We have therefore so far implemented an approximation in our Monte Carlo (MC) code (as have been discussed in [5, 6]), and we will at the end of this section try to sketch the similarities between our implementation and the saturation mechanism in the CGC formalism.

The generic evolution equations for high energy QCD including all possible pomeron interactions are not yet known. Equations have, however, been derived for simple toy models which neglect the complicated topology of the full model [13, 14]. The saturation mechanism in these simpler models have similarities with the CGC formalism, and they can also be formulated in a stochastic evolution with similarities to the dipole evolution in the presence of the dipole swing, as we now explain.

These equations can namely be interpreted in terms of (positive definite) $k \rightarrow k + 1$ vertices [15]. The dipole swing (discussed in more detail below) is a process which instantaneously in Y replaces two initial dipoles, (x_1, y_1) and (x_2, y_2) , with two final dipoles, (x_1, y_2) and (x_2, y_1) . Here $(y)x$ denotes the transverse position of the (anti-)colour end of the dipole (here we do not use boldface letters for the vectors). The generic $k \rightarrow k + 1$ vertices can then be constructed by combining the usual $1 \rightarrow 2$ dipole splitting with $k - 1$ instantaneous dipole swings. In the toy models in [13, 14] these vertices give a boost invariant evolution. However, the amount of information we can extract from the toy models is limited. In QCD it is important to take into account the colour degrees of freedom which are completely absent in the toy models. The colour structures of the multiple scattering diagrams were discussed in detail in [15] and we will here again briefly discuss the colour structures.

The linear cascade evolution is directly related to the leading N_c approximation. The dipole splitting kernel is proportional to $\alpha_s N_c = \bar{\alpha}$ (for simplicity we here neglect the factor π in the definition of $\bar{\alpha}$ as it is completely irrelevant for our discussion), while the scattering diagrams are proportional to $\alpha_s^2 = \bar{\alpha}^2 / N_c^2$. To take into account the effects of multiple scatterings in all frames one would therefore need to include processes proportional to $\bar{\alpha} \cdot \bar{\alpha}^{2n} / N_c^{2n}$ (the first factor of $\bar{\alpha}$ comes from the dipole splitting) in the cascade evolution. In the leading N_c approximation such processes are absent⁴. To correctly include saturation effects in the cascade evolution it is therefore very important that one studies the colour structures of the relevant Feynman diagrams.

⁴The reason one includes multiple scatterings is because they are dominant at high energies even if they are colour suppressed. The contribution from n pomeron exchange goes like $e^{n\omega Y}$ as compared to single pomeron exchange which goes like $e^{\omega Y}$, where ω is the BFKL intercept.

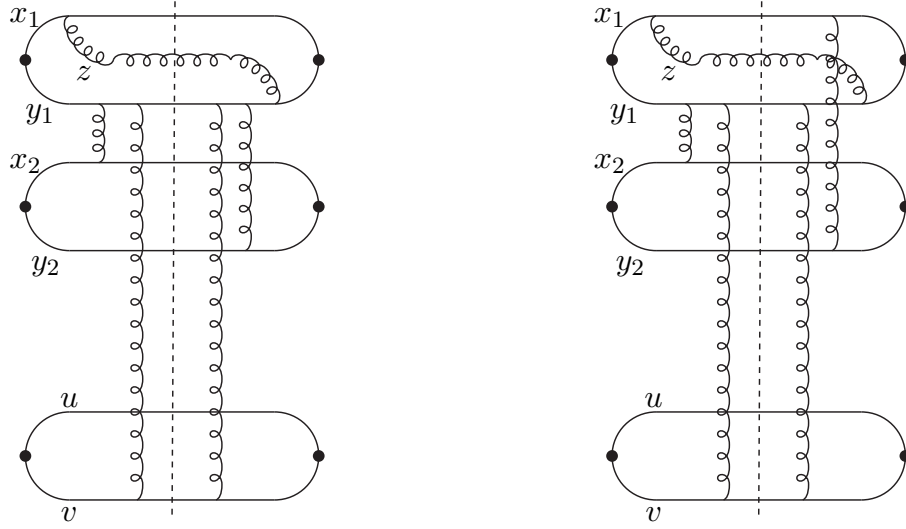


Figure 1: Two diagrams contributing to interactions within the same cascade as explained in the text. The dashed line indicates the cut between the amplitude and the complex conjugate amplitude.

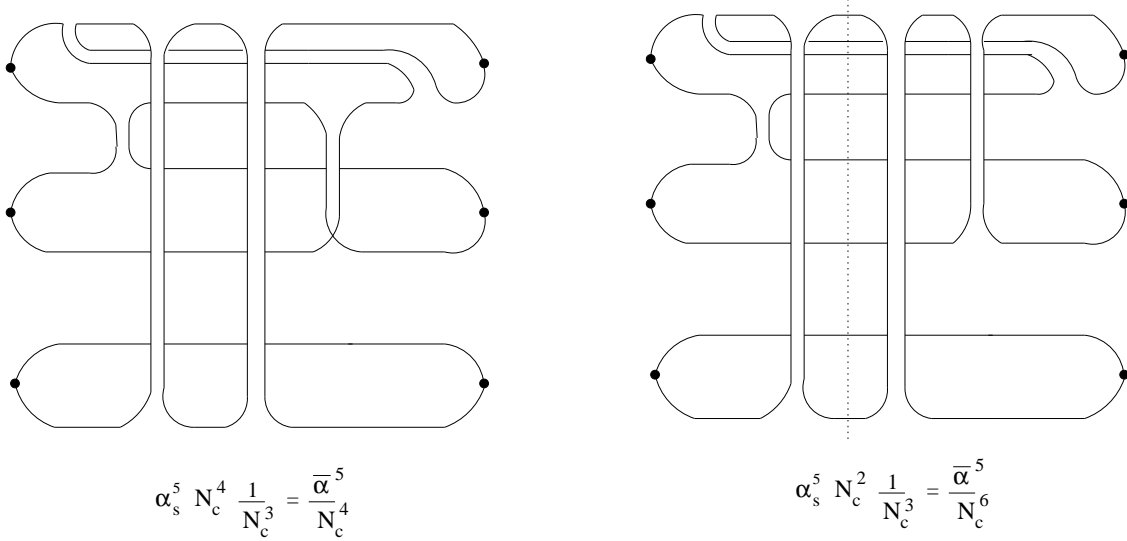


Figure 2: The respective colour structures of the two diagrams from figure 1.

Let us consider the situation in figure 1. Here we have two right moving dipoles, (x_1, y_1) and (x_2, y_2) , and one left moving dipole (u, v) . When rapidity is increased by ΔY , the gluon z can be emitted from (x_1, y_1) (thus we put the evolution into the right moving system). In the left diagram in figure 1 we show just one of the contributions to this process. Here z is in the amplitude emitted by the quark located at x_1 , and is absorbed in the complex conjugate amplitude by the antiquark located at y_1 . In addition to this we have two-gluon exchange between the system consisting of x_1, y_1 and z , and (x_2, y_2) . In

the amplitude a gluon is exchanged between the antiquark at y_1 and the quark at x_2 , while in the complex conjugate amplitude a gluon is exchanged between the antiquark at y_1 and the antiquark at y_2 . These processes contribute to the evolution of the wavefunction of the right moving system. In addition, there is a two-gluon exchange between the right and left moving systems. In the amplitude there is a gluon exchanged between the quark at x_1 and the oppositely moving antiquark at v , and there is again a gluon exchange between x_1 and v in the complex conjugate amplitude. In the right diagram in figure 1, the gluon exchanged between y_1 and y_2 in the complex conjugate amplitude is instead exchanged between x_1 and y_2 .

In figure 2 we show the respective colour structures of the two diagrams from figure 1. Counting the vertices and the colour loops we see that the left diagram is proportional to $\bar{\alpha}^5/N_c^4$. The extra factor $1/N_c^3$ comes from the black dots where we project out the colour singlet contributions (a dipole is a colour singlet). In the right diagram we can count 2 loops, and the process shown is therefore proportional to $\bar{\alpha}^5/N_c^6$ and thus suppressed as compared to the left diagram.

These diagrams contribute to processes which can be interpreted as follows. The left diagram in figure 1 is one of the diagrams which contribute to the process where (x_1, y_1) first splits into (x_1, z) and (y_1, z) by the emission of the gluon z , after which the dipoles (z, y_1) and (x_2, y_2) exchange a gluon, whereby they are replaced by two new dipoles, (z, y_2) and (x_2, y_1) . Then finally the dipole (x_1, z) interacts with the target (u, v) . This process has therefore a dipolar interpretation, and the step where (z, y_1) and (x_2, y_2) are replaced by (z, y_2) and (x_2, y_1) precisely describes the dipole swing. The right diagram in figure 1 can on the other hand not be described in terms of dipoles. Here a gluon is exchanged between (z, y_1) and (x_2, y_2) in the amplitude, but in the complex conjugate amplitude a gluon is instead exchanged between (x_1, z) and (x_2, y_2) . However, we also see that this process is suppressed, since it goes like $\bar{\alpha}^5/N_c^6$ instead of $\bar{\alpha}^5/N_c^4$.

In case the evolution is put into (u, v) , the corresponding diagram to the left diagram in figure 1 would describe a process where (u, v) splits into (u, z) and (z, v) , both of which then scatter against (x_1, y_1) and (x_2, y_2) . This is thus a multiple scattering contribution, referred to as the “fluctuation” contribution in [16]. If one carefully studies all the possible Feynman graphs, then the following picture appears when dipoles in the same cascade are allowed to interact. As mentioned above, first one of the dipoles (x_1, y_1) and (x_2, y_2) splits (say (x_1, y_1)) into two new dipoles. Then one of the two new dipoles swing with (x_2, y_2) , and two newer dipoles are formed. Thus we have three new dipoles at the end of the process. Any one of these three dipoles can then interact with (u, v) . The $2 \rightarrow 3$ vertex which involves the swing goes like $\bar{\alpha}^3/N_c^2$, and is therefore colour suppressed. There are also terms which cannot be interpreted in terms of dipole interactions. However, these are all proportional to $\bar{\alpha}^3/N_c^4$ and they can therefore be neglected as compared to the dipole swing contribution. It was shown in [15] that the colour structures of all the multiple scatterings diagrams exactly correspond to the colour structures of diagrams which in the evolution of a dipole cascade can be interpreted in terms of the dipole swing and the $k \rightarrow k + 1$ vertices mentioned above. Whether or not one can thereby obtain a boost invariant evolution is, however, not quite clear. A detailed study trying to attack this problem, and to study the

structure of the generated evolution equations is under way [17].

Boost invariance (sometimes referred to as the self-duality) of the evolution, and the generalization of the B-JIMWLK hierarchy, have previously been discussed in a series of papers [16, 18–20]. Note, however, that the $k \rightarrow k + 1$ vertices mentioned above give rise to equations more general than the “Pomeron Loop” equations derived in [16, 20] (the toy model analogy of this has been discussed for example in [14]). As mentioned, it is, however, not known whether or not one can obtain a boost invariant evolution in the full model. For example, in [21] it was shown that the higher order corrections arising from the strong classical fields in the JIMWLK formalism contains quadrupoles, sextupoles and so on. It may therefore be that one needs to include more complicated colour structures in a fully consistent formalism.

In the MC implementation of our model [5, 6], each dipole is given one of N_c^2 possible colour indices, and only dipoles with the same colour index are allowed to swing⁵. Here the weight for the swing process was chosen so that it favours the formation of smaller dipoles, which explicitly introduces saturation effects in the cascade evolution as smaller dipoles both split and interact more weakly. As we discussed in [5] this procedure also approximates higher order multipoles, which might be needed in a consistent formulation as mentioned above. The similarity with the CGC formalism can then be explained as follows. In the CGC, it can be shown that the number density of gluons satisfy [2]

$$\frac{dN}{dY d^2\mathbf{b} d^2\mathbf{k}} \lesssim \frac{1}{\alpha_s} \quad (2.7)$$

due to saturation. If one integrates over rapidity, one rather gets

$$\frac{dN}{d^2\mathbf{b} d^2\mathbf{k}} \lesssim \frac{1}{\alpha_s^2}. \quad (2.8)$$

What happens in the CGC is that one can continue to pack the hadron with more gluons until there are so many gluons overlapping that their mutual interaction is strong enough to prevent further occupation at a particular \mathbf{b} . In a semiclassical picture we can think of each gluon as a disc of radius $\sim 1/|\mathbf{k}|$. Holding \mathbf{k} fixed, one will sooner or later reach a point where it is not possible to put in any more gluons of that \mathbf{k} . In that case we have to increase \mathbf{k} , which corresponds to adding smaller discs into the proton. At one stage those smaller discs will also fill up the available holes, but there is then more room for even smaller discs and so on. One can continue in this way forever, with the typical gluon momenta being pushed to higher values, and the total number of gluons therefore never ceases to grow⁶.

The dipole swing works in a very similar way. Since the evolution is driven by the $1 \rightarrow 2$ splitting plus the $2 \rightarrow 2$ swing, the total number of dipoles will continue to grow forever. Assume, however, that we wish to put many dipoles of similar size \mathbf{r} around the same impact parameter \mathbf{b} . If the number of dipoles is less than N_c^2 , there are no problems since the swing is not very likely. However, as soon as we have N_c^2 dipoles they can start

⁵The probability that a given colour–anti-colour pair forms a colour singlet is $1/N_c^2$.

⁶The production rate of additional gluons does saturate however.

to swing, and since in this case they almost sit on top of each other, they will do so as soon as the chance is given (the swing favours the formation of smaller dipoles, and in this case the swing probability is thus very large [5]). When two dipoles swing they will be replaced by two smaller dipoles, with different impact parameters \mathbf{b}' . This implies that the dipole occupation number satisfies

$$\frac{dN}{d^2\mathbf{b}d^2\mathbf{r}} \lesssim N_c^2 \sim \frac{1}{\alpha_s^2}. \quad (2.9)$$

Here we assume $\bar{\alpha}$ to be fixed and of order $1/\pi$, in which case we get $\alpha_s \sim 1/N_c$. When the number of smaller dipoles around \mathbf{b}' gets large enough they will in turn start to swing to produce even smaller dipoles and so on. Thus we get a picture which is similar to that in the CGC formalism.

The dipole swing suppresses the growth of the cascade in the transverse plane, and it is interesting to see how large effects it has on the evolution. In the next section we will therefore present our results with and without the swing. Obviously, we cannot expect the swing to change the Y dependence of $R_{bd}(Y)$ in a qualitative manner, in particular we cannot expect it to modify an exponential growth, since the associated interactions are still mediated by massless gluons.

3. Results

We will in this section present the results obtained from our MC simulation for the growth of $R_{bd}(Y)$. Let us first mention that it is extremely difficult to make analytic predictions as in section 2.1. In our simulations we take into account effects of energy-momentum conservation, which are related to, but go beyond, the next-to-leading order corrections to the cascade evolution. As mentioned in the previous section, we also include saturation effects in the evolution, and the full equations which include these effects are not known (even in the large N_c limit), and once they are known they will probably be extremely complicated to solve. Furthermore, analytic estimates can never fully take into account the full impact parameter dependence of the evolution, which is relevant for the present study.

The first results we show are for the case of a running coupling, and without any confinement effects. In order to avoid singularities, the value of $\alpha_s(p_\perp)$ is frozen below the scale $p_\perp = 2/r_{max}$ where r_{max} is a free parameter which in our full model sets the confinement scale. In our previous studies [6] we have set $r_{max} = 3.5 \text{ GeV}^{-1}$ which is also the value we will use in the present study. (Λ_{QCD} is fixed to 0.22 GeV)

In the discussion in section 2.1, we considered the projectile to be an elementary dipole. Due to the fact that higher Y values are extremely time consuming to simulate, we will here use a projectile which is more dense initially. We will therefore consider pp scattering where the initial proton is modeled as consisting of three dipoles (with a Gaussian distribution in sizes determined by the scale r_{max}) in a triangular configuration as was discussed in [5, 6], where the frame independence of the process have also been demonstrated. We will therefore compute $T_Y(\mathbf{b})$ in the CM frame, since this is numerically the least time consuming frame.

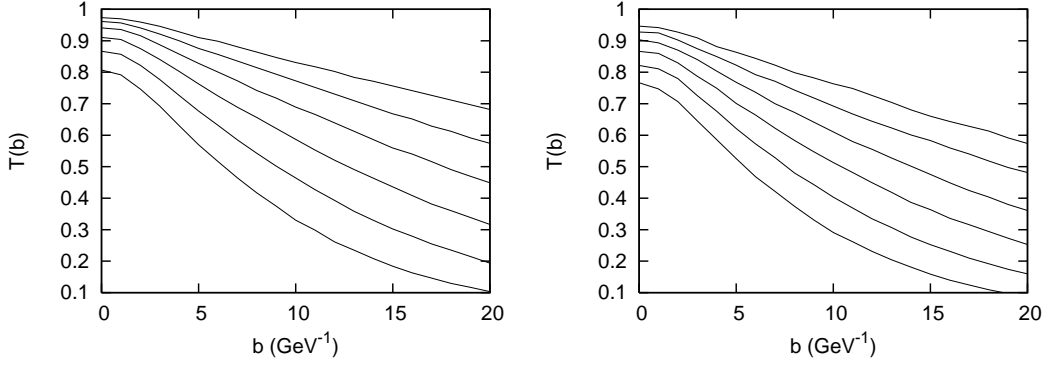


Figure 3: The transverse profile of the scattering amplitude T including a running coupling, and without confinement effects. The left figure excludes the swing while the right figure includes it. In both figures the lowest curve is calculated at $Y = 8$, and Y is increased by 2 units for each new curve. In both cases an exponential growth of $R_{bd}(Y)$ is seen. The main mechanism driving the growth is clearly the very fast growth of the white region.

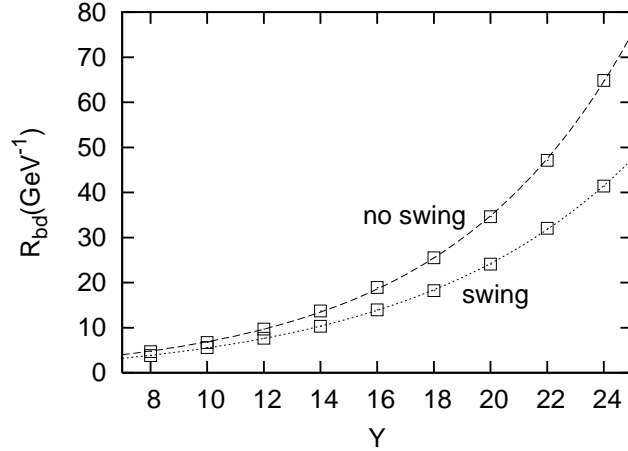


Figure 4: The black disc radius $R_{bd}(Y)$ plotted as a function of Y , as calculated from figure 3. The squares correspond to evolution including (lower set), and excluding (upper set) the swing. Together with each curve, the corresponding fits are also shown.

Our first result are shown in figure 3. Here we plot $T_Y(b)$ as a function of b (we average over the angle). We show two plots, including (right plot) and excluding (left plot) the swing. The lowest curves are calculated at $Y = 8$, and Y is increased by 2 units for each new curve. We see very large contributions from large impact parameters, and the resulting profile is very flat. In this case $R_{bd}(Y)$ grows exponentially which can be seen in figure 4. Here, the upper curve excludes the swing, and we find that $R_{bd}(Y)$ can be fitted as $R_{bd}(Y) \approx 1.8 \cdot \exp(0.15Y) \text{ GeV}^{-1}$. If the dipole swing is included we instead get $R_{bd}(Y) \approx 2.0 \cdot \exp(0.13Y) \text{ GeV}^{-1}$. Also in the case where we include the swing, we see that $R_{bd}(Y)$ grows very rapidly. As mentioned in the introduction this is partly due to the breakdown of perturbation theory since the value $\alpha_s(p_\perp)$ is very large during the evolution, which is moreover extremely sensitive to the infrared cutoff r_{max} .

Of course, since in this case the initial dipoles are rather large (with sizes close to

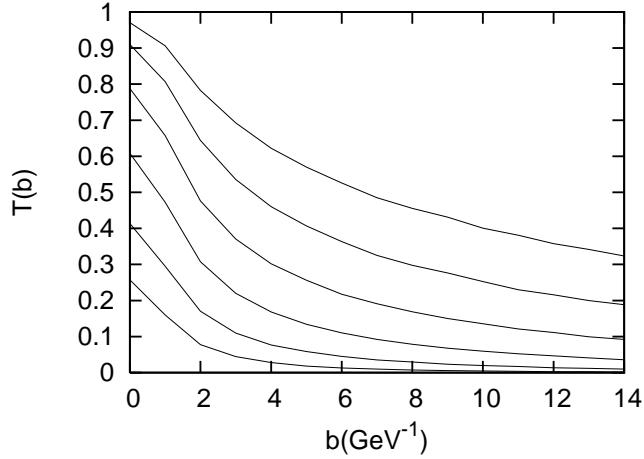


Figure 5: The transverse profile of T for onium-onium scattering, without the swing. We again find a very flat profile, with very large contributions from large b . The lowest curve is calculated at $Y = 12$, and Y is increased by 4 units for each new curve.

r_{max}) one is in the soft region already from the beginning. We therefore also study onium-onium scattering, where the initial onia have small sizes, we take the two cases $r_0 = 0.5$ and 1 GeV^{-1} respectively (both initial onia have the same size). In figure 5 we show the transverse profile for the case $r_0 = 1 \text{ GeV}^{-1}$. Here we do not include the swing and we once again find a very flat distribution implying an exponential growth for $R_{bd}(Y)$. The result for the case $r_0 = 0.5 \text{ GeV}^{-1}$ looks essentially the same.

Next we switch to a fixed coupling, $\alpha_s = 0.2$. It is well known that the leading order dipole cascade also in this case shows a fast diffusion towards large dipole sizes. In [4] we demonstrated the very large effects of energy-momentum conservation on the evolution. In this case the production of both small (from p_+ conservation) and large (from p_- conservation) dipoles are suppressed, and the growth of the cross section is severely dampened.

The transverse profile of the scattering amplitude is shown in figure 6. As compared to figure 3 we see that the growth is significantly reduced. This is because the unrealistically large contributions from larger b present in the running coupling case are much reduced. From figure 6 it seems that, for rapidities under $Y \approx 20$, the growth is even linear⁷. However, as Y increases, we clearly see a deviation from the linear growth, which becomes greater for the largest Y . Clearly, the FM bound-breaking growth arises not because the central regions reach the black disc limit too fast, but rather because the white region, where the scattering is very weak initially, turns grey too fast. This indeed confirms the expectation that the FM bound is in this case violated due to long range contributions coming from the perturbative Coulomb fields [8]. What is interesting, however, is the fact that the growth of $R_{bd}(Y)$ is much slower than expected from the leading order evolution. This is clearly illustrated in figure 7. What we see here is that the shape of $R_{bd}(Y)$ cannot be

⁷In order to see the FM bound-breaking growth sooner, we have here defined R_{bd} for $a = 0.3$ in (2.1). This will of course affect the absolute value of R_{bd} , but it does not change the fact that R_{bd} grows more than linearly with Y .

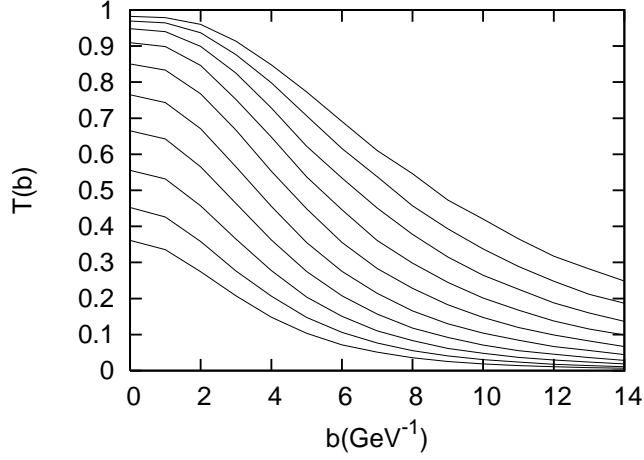


Figure 6: The transverse profile of the scattering amplitude for a fixed coupling, $\alpha_s = 0.2$. In this case the swing is not included. The lowest curve is calculated at $Y = 8$, and Y is increased by 2 units for each successive curve. Although the growth of $R_{bd}(Y)$ seems to be linear for lower Y , we can see that the white region grows very fast, implying an increasingly faster growth of $R_{bd}(Y)$ as Y increases.

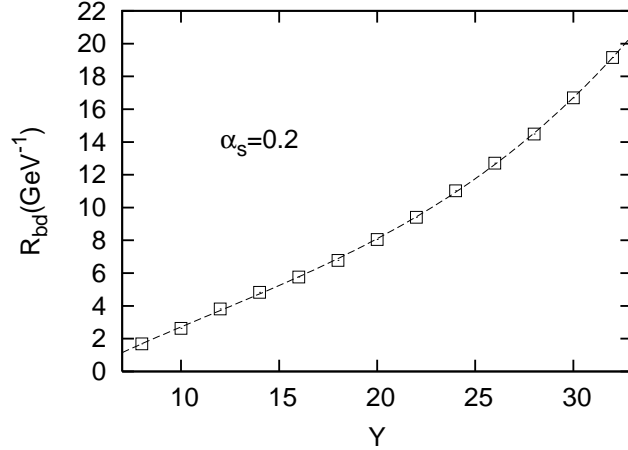


Figure 7: The black disc radius $R_{bd}(Y)$ as a function of Y as calculated from figure 6 (squares). In this case $R_{bd}(Y)$ can be fitted by a polynomial (the dashed line) as explained in the text.

fitted by an exponential, at least for Y up to 32. The growth accelerates as Y increases, so as $Y \rightarrow \infty$ the growth should eventually reach an exponential (indeed the white region already grows exponentially). For the present values we instead find that the shape can be fitted by a polynomial, and in figure 7 we show a fit $R = (-3.3 + 0.76 \cdot Y - 0.02 \cdot Y^2 + 6 \cdot 10^{-4} \cdot Y^3) \text{GeV}^{-1}$, which is the best fit we have found. Such a fit would imply a cross section growing like $\sigma_{tot} \sim \ln^6(s/s_0)$. This growth is further reduced if we include the dipole swing, as we illustrate in figures 8 and 9. Even if the growth seems to be linear, one can again see that the white region expands rapidly and the growth of R_{bd} accelerates as Y increases. The fit in figure 9 corresponds to a quadratic fit.

In order to satisfy the FM bound we must introduce a scale above which the gluon fields

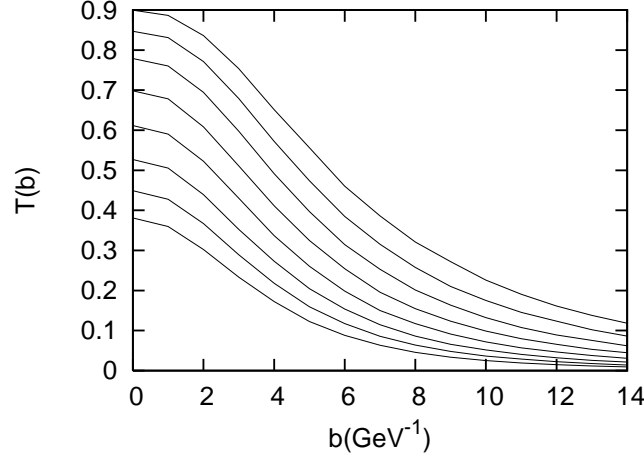


Figure 8: The transverse profile for fixed coupling and including the swing. The lowest curve is calculated at $Y = 10$ and Y is increased 2 units for each new curve.

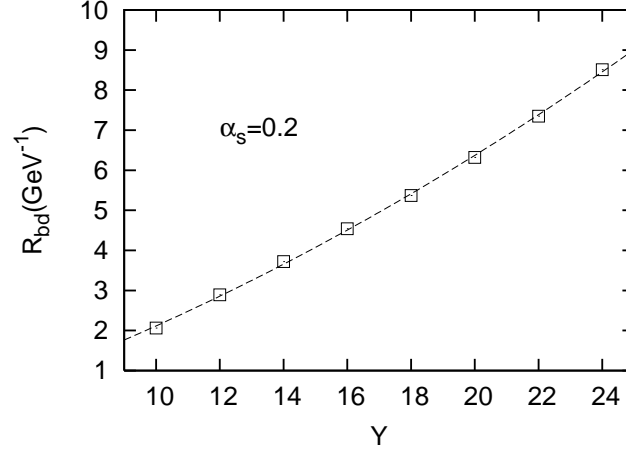


Figure 9: The black disc radius $R_{bd}(Y)$ as a function of Y as calculated from figure 8

falls off exponentially. In [6] we replaced the momentum space Coulomb propagators, $1/\mathbf{k}^2$, by screened propagators, $1/(\mathbf{k}^2 + M^2)$, where $M = 1/r_{max}$. The dipole splitting kernel, for the process $(\mathbf{x}, \mathbf{y}) \rightarrow (\mathbf{x}, \mathbf{z}) + (\mathbf{z}, \mathbf{y})$, is then modified as

$$\frac{(\mathbf{x} - \mathbf{y})^2}{(\mathbf{x} - \mathbf{z})^2 (\mathbf{z} - \mathbf{y})^2} \rightarrow \left(\frac{1}{r_{max}} \frac{\mathbf{x} - \mathbf{z}}{|\mathbf{x} - \mathbf{z}|} K_1(|\mathbf{x} - \mathbf{z}|/r_{max}) - \frac{1}{r_{max}} \frac{\mathbf{z} - \mathbf{y}}{|\mathbf{z} - \mathbf{y}|} K_1(|\mathbf{z} - \mathbf{y}|/r_{max}) \right)^2. \quad (3.1)$$

Similarly the dipole-dipole scattering amplitude $T_0(\mathbf{x}, \mathbf{y}|\mathbf{u}, \mathbf{v})$ is modified as

$$\frac{\alpha_s^2}{2} \ln^2 \left\{ \frac{|\mathbf{x} - \mathbf{v}| |\mathbf{y} - \mathbf{u}|}{|\mathbf{x} - \mathbf{u}| |\mathbf{y} - \mathbf{v}|} \right\} \rightarrow \frac{\alpha_s^2}{2} \left(K_0(|\mathbf{x} - \mathbf{u}|/r_{max}) - K_0(|\mathbf{x} - \mathbf{v}|/r_{max}) - K_0(|\mathbf{y} - \mathbf{u}|/r_{max}) + K_0(|\mathbf{y} - \mathbf{v}|/r_{max}) \right)^2. \quad (3.2)$$

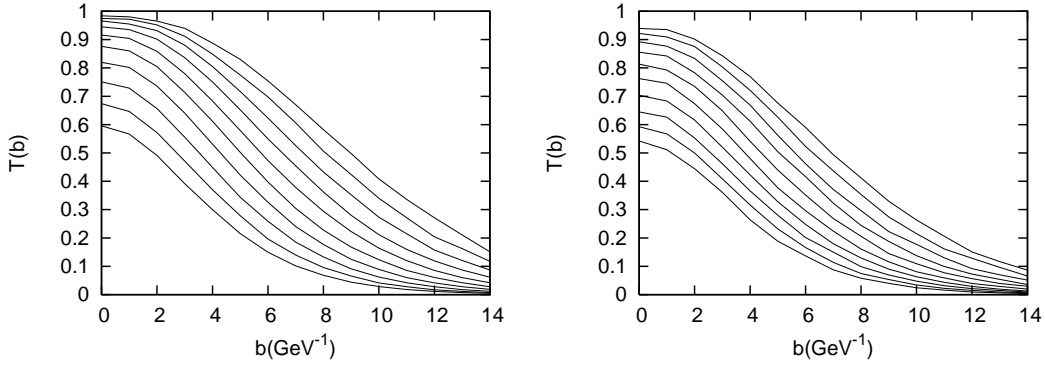


Figure 10: The transverse profile of T including confinement effects via equations (3.1) and (3.2). In the left figure the swing is excluded while it is included in the right figure. The lowest curves are calculated at $Y = 8$, and Y is increased by 2 units for each new curve. Here the growth is clearly linear, and as expected we see that the growth of the white region is considerably suppressed.

Here K_0 and K_1 are modified Bessel functions which both behave as $K(x) \sim \sqrt{\frac{2}{x}} e^{-x}$ for large x . In the analysis of section 2.1, this would imply an exponentially decaying profile in \mathbf{b} , which would compensate the exponential growth in Y of the BFKL solution. The evolution should then satisfy the FM bound. This has been used in [7] to estimate the constant C in (1.1) as

$$C = 2\pi \left(\frac{\omega}{\mu} \right)^2, \quad (3.3)$$

where ω was defined in (2.4), and μ is the confinement scale, *i.e.* r_{max}^{-1} in our model. The constant C can thus roughly be determined by combining the hard pomeron intercept with the non-perturbative confinement scale, albeit in a heuristic fashion.

Recently it has been shown that experimental results on pp collisions favours a $\ln^2 s$ fit (rather than a $\ln s$ fit) to the total pp cross section [22]. The fit in [22] has the form

$$\sigma \approx c_0 + c_1 \ln \left(\frac{s}{2m^2} \right) + c_2 \ln^2 \left(\frac{s}{2m^2} \right), \quad (3.4)$$

where we have neglected terms which fall off as a power of s . The various coefficients above were found to be $c_0 \approx 37$ mb, $c_1 \approx -1.4$ mb and $c_2 \approx 0.28$ mb. In [7], the value of μ has been argued to be around $2m_\pi \approx 0.28$ GeV, which interestingly is equal to r_{max}^{-1} with $r_{max} = 3.5$ GeV $^{-1}$. In this case the value of (3.3) would be around 9 mb, considerably higher than c_2 above. Of course, the value of (3.3) is not supposed to reproduce c_2 since it has been derived under rather crude assumptions (any attempt to include nonperturbative effects will admittedly be heuristic as well). It is also a well known fact that the leading order BFKL exponent ω is too large to fit data. If we would for example replace ω by its NLO value, $\omega \approx 0.3$, C would be reduced almost by a factor of 4.

In figure 10 we show the transverse profile of the scattering amplitude, calculated using (3.1) and (3.2), and using a running coupling. Note that, as compared to figure 6, the difference now is that the growth of the white region is considerably suppressed, as expected from confinement. In this case we can see a linear growth, which is illustrated in

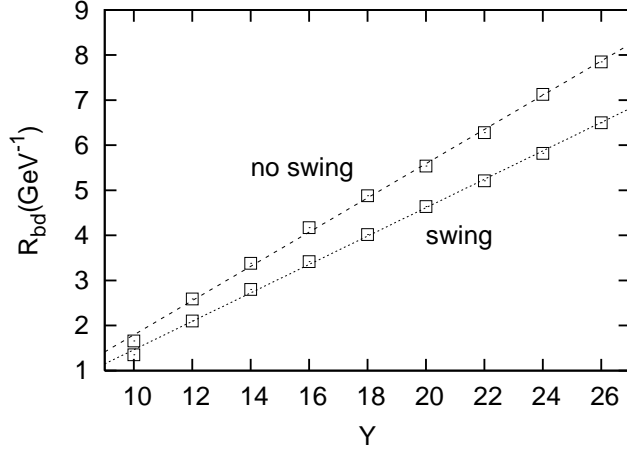


Figure 11: The black disc radius $R_{bd}(Y)$ calculated from figure 10 excluding (upper set of squares) and including (lower set of squares) the swing. Lines represent linear fits to the squares.

figure 11. Here we find that R_{bd} can be fitted as $R_{bd}(Y) = (-1.36 + 0.39Y)\text{GeV}^{-1}$ when the swing is excluded, and as $R_{bd}(Y) = (-1.70 + 0.31Y)\text{GeV}^{-1}$ when it is included. This would imply a cross section growing as $\sigma \sim 2\pi \cdot 0.39^2 \ln^2 s \text{ GeV}^2 = 0.37 \cdot \ln^2 s \text{ mb}$ for the former case, while for the latter case we would have $\sigma \sim 2\pi \cdot 0.31^2 \ln^2 s \text{ GeV}^2 = 0.24 \cdot \ln^2 s \text{ mb}$. The results are indeed quite close to the c_2 term in (3.4). We might also ask how good the approximation $\sigma \sim 2\pi R_{bd}^2(Y)$ is. The MC results for the transverse profiles in figure 10 can be estimated rather well (for fixed Y) by simple Gaussians, $T = T(0) \exp(-c \cdot b^2)$. Thus, approximating these curves by such functions⁸ the cross section would be given by

$$\sigma_1 = 2 \int d^2\mathbf{b} T(0) \exp(-c \cdot b^2) = \frac{\pi}{c} T(0). \quad (3.5)$$

On the other hand, R_{bd} is defined as $T(R_{bd}) = a$ with $a = \mathcal{O}(0.5)$, and the approximation $\sigma \sim 2\pi R_{bd}^2(Y)$ then gives

$$\sigma_2 = \frac{2\pi}{c} \ln\left(\frac{T(0)}{a}\right). \quad (3.6)$$

Thus

$$\frac{\sigma_2}{\sigma_1} = \frac{2}{T(0)} \ln\left(\frac{T(0)}{a}\right). \quad (3.7)$$

For the Tevatron for example, we have $T(0) \approx 0.7$, while in figure 11 we have set $a \approx 0.6$. This would give $\sigma_2/\sigma_1 \approx 0.5$. For higher energies where $T(0) \rightarrow 1$ we get $\sigma_2/\sigma_1 \approx 1$ so that the approximation $\sigma \sim 2\pi R_{bd}^2(Y)$ works reasonably well.

Of course we might as well directly calculate the total cross section using the MC, such as we did in [6]. Thus we can try to fit a curve of the form (3.4) to our results [6] for the

⁸Given the fact the functions K_1 in the kernel (3.1) fall exponentially one might think that an exponential function would better approximate the b -profile. The good Gaussian approximation is related to our initial proton model which has a Gaussian distribution [6]. Actually our b -profile has a somewhat longer tail than a Gaussian for large b due to the fluctuations in the evolution, as was discussed in [6].

total pp cross section. We thus parameterize the cross section as

$$\sigma = A + B \ln s + C \ln^2 s, \quad (3.8)$$

where s is measured in units of GeV^2 . In this case we find the results $A = 34 \text{ mb}$, $B = -1.8 \text{ mb}$ and $C = 0.30 \text{ mb}$ which are quite close to the values c_0 , c_1 and c_2 in (3.4). We also try a fit $\sigma = D + E \ln^2 s$ which works equally well, and we find $D = 20 \text{ mb}$ and $E = 0.24 \text{ mb}$. We thus find that the Froissart bound is saturated, and by combining the perturbative evolution with nonperturbative confinement effects we moreover obtain a value for C which is consistent with data.

4. Conclusions

We have in this paper studied the growth of the black disc radius $R_{bd}(Y)$ for hadronic collisions, using our model developed in [4–6]. Using a purely perturbative approach one cannot expect the FM bound to be satisfied, and for the running coupling case we indeed find an exponential growth for $R_{bd}(Y)$. On the other hand when a fixed coupling is used we again find a fast growth of $R_{bd}(Y)$, but the growth is in this case not an exponential as in the running coupling case, but can be fitted by a polynomial (at least for rapidities up to 32 units, corresponding to $s \sim 10^{14} \text{ GeV}^2$). This is due to our inclusion of energy-momentum conservation effects in the evolution, which severely dampens the leading order growth. However, it can be seen that the white region expands exponentially, which should imply an exponential growth for $R_{bd}(Y)$ eventually. The fact that the running coupling case shows such a fast growth is because, without any suppression of large dipoles, the coupling gets very large during the evolution. Moreover, one gets unrealistically large contributions from large transverse separations.

We model confinement effects by replacing the Coulomb propagators by screened propagators, in which case $R_{bd}(Y)$ grows linearly with Y , implying that the FM bound is actually saturated. Furthermore, including saturation effects during the cascade evolution, we see that we obtain a value for the coefficient C in (1.1) which is consistent with data.

Obviously, our specific model used here makes sense only when including nonperturbative effects since the initial dipoles in the proton are quite large. However, also in the case where we start from a, smaller, single dipole did we see a very fast growth. It is also interesting to see what would happen if one starts with a system containing perturbative dipoles, which is at the same time quite dense. Then we would expect saturation to slow down the evolution, although we will of course still get an exponential growth if no confinement effects are included. An interesting initial model is a proton consisting of three “hot spots”, *i.e.* three saturated spots inside the proton. This model was discussed in [9]. The sizes of these spots, related to the scale of chiral symmetry breaking, is estimated to be around 0.3 fm. Thus one may at least initially neglect confinement effects for the evolution of each spot.

To test the sensitivity of our model to the initial assumptions, we have also tried a model where the proton initially consists of 6 dipoles in 3 spots (2 dipoles in each spot), where each spot has a size around 0.3 fm. Including the swing, and with a running coupling

and no confinement effects, we again find a very fast growth of σ_{tot} . For spot sizes of around 0.3 fm, we find that the cross section shows a $s^{0.21}$ behaviour.

Finally, when confinement is included we find that a fit $D + E \cdot \ln^2 s$ gives, $E \approx 0.31\text{mb}$ which is higher than the result 0.24 mb found above. However, we should mention that this initial model also reproduces the available high energy data rather well. Furthermore we also get good results, as in [6], for the diffractive and elastic cross sections, both in pp collisions and in DIS. To the accuracy of our model, we therefore get a reasonable description of data also with such an initial model.

Acknowledgments

I am grateful to Gösta Gustafson for his encouragement and support when this work was initiated in Lund. I would also like to thank Edmond Iancu for his critical remarks and for helpful discussions.

References

- [1] I. Balitsky *Nucl. Phys.* **B463** (1996) 99–160, [hep-ph/9509348](#).
- [2] E. Iancu, A. Leonidov, and L. McLerran [hep-ph/0202270](#).
- [3] A. H. Mueller *Nucl. Phys.* **B415** (1994) 373–385.
- [4] E. Avsar, G. Gustafson, and L. Lönnblad *JHEP* **07** (2005) 062, [hep-ph/0503181](#).
- [5] E. Avsar, G. Gustafson, and L. Lönnblad *JHEP* **01** (2007) 012, [hep-ph/0610157](#).
- [6] E. Avsar, G. Gustafson, and L. Lönnblad *JHEP* **12** (2007) 012, [arXiv:0709.1368 \[hep-ph\]](#).
- [7] E. Ferreira, E. Iancu, K. Itakura, and L. McLerran *Nucl. Phys.* **A710** (2002) 373–414, [hep-ph/0206241](#).
- [8] A. Kovner and U. A. Wiedemann *Phys. Lett.* **B551** (2003) 311–316, [hep-ph/0207335](#).
- [9] A. Kovner and U. A. Wiedemann *Phys. Rev.* **D66** (2002) 034031, [hep-ph/0204277](#).
- [10] T. Ikeda and L. McLerran *Nucl. Phys.* **A756** (2005) 385–398, [hep-ph/0410345](#).
- [11] Y. V. Kovchegov *Phys. Rev.* **D60** (1999) 034008, [hep-ph/9901281](#).
- [12] K. J. Golec-Biernat and A. M. Stasto *Nucl. Phys.* **B668** (2003) 345–363, [hep-ph/0306279](#).
- [13] J. P. Blaizot, E. Iancu, and D. N. Triantafyllopoulos *Nucl. Phys.* **A784** (2007) 227–258, [hep-ph/0606253](#).
- [14] E. Iancu, J. T. de Santana Amaral, G. Soyez, and D. N. Triantafyllopoulos *Nucl. Phys.* **A786** (2007) 131–163, [hep-ph/0611105](#).
- [15] E. Avsar *JHEP* **11** (2007) 027, [arXiv:0709.1371 \[hep-ph\]](#).
- [16] E. Iancu and D. N. Triantafyllopoulos *Phys. Lett.* **B610** (2005) 253–261, [hep-ph/0501193](#).
- [17] E. Avsar. Work under progress.
- [18] A. Kovner and M. Lublinsky *Phys. Rev. Lett.* **94** (2005) 181603, [hep-ph/0502119](#).
- [19] Y. Hatta, E. Iancu, L. McLerran, A. Stasto, and D. N. Triantafyllopoulos *Nucl. Phys.* **A764** (2006) 423–459, [hep-ph/0504182](#).
- [20] E. Levin and M. Lublinsky *Nucl. Phys.* **A763** (2005) 172–196, [hep-ph/0501173](#).
- [21] J. L. Albacete, N. Armesto, and J. G. Milhano *JHEP* **11** (2006) 074, [hep-ph/0608095](#).
- [22] M. M. Block and F. Halzen *Phys. Rev.* **D72** (2005) 036006, [hep-ph/0506031](#).